

# 3D Point Cloud Generation via Autoregressive Up-sampling

Ziqiao Meng<sup>1,2</sup> Qichao Wang<sup>1</sup> Zhipeng Zhou<sup>3</sup> Irwin King<sup>2</sup> Peilin Zhao<sup>1</sup>  
<sup>1</sup> Tencent AI Lab <sup>2</sup> The Chinese University of Hong Kong <sup>3</sup> Nanyang Technological University

## Abstract

We introduce a pioneering autoregressive generative model for 3D point cloud generation. Inspired by visual autoregressive modeling (VAR), we conceptualize point cloud generation as an autoregressive up-sampling process. This leads to our novel model, **PointARU**, which progressively refines 3D point clouds from coarse to fine scales. PointARU follows a two-stage training paradigm: first, it learns multi-scale discrete representations of point clouds, and then it trains an autoregressive transformer for next-scale prediction. To address the inherent unordered and irregular structure of point clouds, we incorporate specialized point-based up-sampling network modules in both stages and integrate 3D absolute positional encoding based on the decoded point cloud at each scale during the second stage. Our model surpasses state-of-the-art (SoTA) diffusion-based approaches in both **generation quality** and **parameter efficiency** across diverse experimental settings, marking a new milestone for autoregressive methods in 3D point cloud generation. Furthermore, PointARU demonstrates exceptional performance in completing partial 3D shapes and up-sampling sparse point clouds, outperforming existing generative models in these tasks.

## 1. Introduction

The 3D point cloud is a fundamental data representation for 3D object shapes, describing an object as a collection of points, each defined by its 3D coordinates. This format is easily obtained through laser scanning and efficiently stores high-quality geometric information. Developing effective point cloud generative models is essential for capturing the underlying distribution of 3D shapes, enabling advancements in various downstream tasks such as point cloud up-sampling [45], completion [12, 22], and synthesis [41]. However, generating high-quality point clouds remains challenging due to the complex geometry and irregular structure inherent in these data sets.

The recent remarkable success of large language models [28, 29] has reignited interest in autoregressive generative modeling across various domains. This breakthrough has

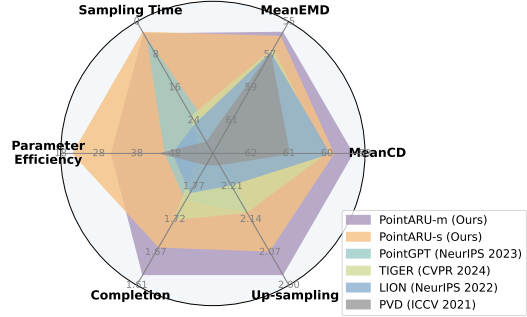


Figure 1. The overall performance comparison between our PointARU and several recent strong baseline methods.

spurred numerous efforts to extend autoregressive modeling to other modalities, including images [4, 16, 19, 38], audio [39, 47], and even unified multi-modal learning [42, 48]. However, its application to 3D point cloud generation remains largely unexplored. The unstructured and irregular nature of 3D point clouds presents a significant challenge in defining a clear sequential order for generating a set of 3D points. Several strategies have been proposed to address this issue. PointGrow [37] establishes a generation order by sorting points based on their  $z$ -axis coordinates. ShapeFormer [43] converts point clouds into voxel grids, flattening the learned codebook embeddings into sequences using a row-major order. PointVQVAE [6] introduces a canonical mapping by projecting each patch onto a sphere and serializing the points in a spiral order. AutoSDF [26] represents point clouds as randomly permuted sequences of latent variables, while PointGPT [5] leverages the Morton code ordering to impose structure on inherently disordered points. Although these approaches have achieved promising empirical results, they still lag behind state-of-the-art (SoTA) diffusion-based methods [25, 35, 46, 49] in terms of generation quality.

In this study, we introduce PointARU, a novel autoregressive generative model for 3D point cloud generation. Drawing inspiration from visual autoregressive modeling (VAR) in 2D image generation [38], PointARU adopts a coarse-to-fine strategy, progressively refining point clouds through next-scale prediction. Compared to traditional se-

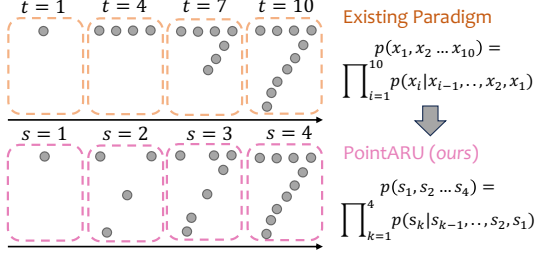


Figure 2. The illustration uses a two-dimensional point cloud as an example. Unlike existing autoregressive generation paradigms that define a fixed generation order, PointARU follows a scale-by-scale approach, progressively generating the entire point cloud from coarse to fine.

quential generation methods, PointARU offers *two key advantages*. First, it eliminates the need for a fixed generation order, which is inherently ambiguous in unordered point clouds. Second, it enables full spatial correlation by generating all points simultaneously at each scale, effectively capturing the spatial dependencies of 3D points.

Specifically, PointARU reinterprets point cloud generation as an iterative up-sampling process, as illustrated in Figure 2, and follows a two-stage training approach. In the first stage, we design a multi-scale autoencoder to learn discrete token representations of point clouds at different scales using residual vector quantization [16]. To accommodate the irregular nature of point clouds, we integrate specialized down-sampling and up-sampling operations within the multi-scale autoencoder. In the second stage, we develop a multi-scale autoregressive point cloud transformer to model the sequential generation of tokens from coarse to fine. To incorporate geometric inductive bias and enhance learning efficiency, we introduce a local attention masking strategy within each scale, encoding prior distance information between point pairs. Additionally, we apply absolute 3D positional encoding, leveraging decoded intermediate-scale point cloud structures to provide the model with precise spatial awareness.

We conduct extensive experiments on the ShapeNet benchmark dataset under diverse settings to demonstrate the superiority of PointARU. In the standard single-class setting, PointARU achieves state-of-the-art (SOTA) generation quality across three fundamental categories, attaining the lowest average Chamfer Distance (Mean CD) and Earth Mover’s Distance (Mean EMD), marking a new milestone for autoregressive modeling. Furthermore, compared to strong diffusion-based baselines, PointARU exhibits significantly **higher parameter efficiency** and **faster sampling speed**, underscoring its scalability. In the more challenging multi-class setting, PointARU also achieves SOTA performance, demonstrating its capability in cross-category learning. Owing to its design principles, PointARU significantly

outperforms baseline methods in downstream tasks such as partial point cloud completion and point cloud up-sampling. Our contributions can be summarized as follows:

- We introduce PointARU, a novel autoregressive model for 3D point cloud generation that employs autoregressive up-sampling, eliminating the need to explicitly define the point generation order as required in previous approaches;
- We conduct extensive experiments on the ShapeNet dataset across diverse settings and downstream tasks. Empirical results demonstrate that PointARU achieves SoTA generation quality while offering high scalability.

## 2. Related Works

**Point Cloud Generation.** Deep generative models have made significant advances in 3D point cloud generation. For instance, PointFlow [44] models the latent distribution of point clouds using a continuous normalizing flow. Further progress has been achieved by models such as DPM [25], ShapeGF [2], PVD [49], LION [46], and TIGER [35], which leverage denoising diffusion probabilistic models to generate 3D point clouds by applying a denoising process to inputs or latent representations in a continuous space. Some studies [36, 40] have sought to improve the sampling efficiency of diffusion-based approaches by incorporating straight flows or ODE solvers. However, experimental results indicate that these methods frequently introduce a trade-off, leading to suboptimal generation quality. In contrast, autoregressive point cloud generation models [5, 6, 37] have received comparatively less attention due to their historically inferior performance relative to diffusion-based methods. In this work, we introduce PointARU, a novel autoregressive model that achieves state-of-the-art point cloud generation quality with high parameter efficiency and competitive inference speed, unlocking new possibilities in this domain.

**Point Cloud Up-sampling.** Point cloud up-sampling is a crucial process in 3D modeling, aimed at increasing the resolution of low-resolution 3D point clouds. PU-Net [45] pioneered the use of deep neural networks for this task, laying the foundation for subsequent advancements. Models such as PU-GCN [30] and PU-Transformer [33] have further refined point cloud feature extraction by leveraging graph convolutional networks and transformer networks, respectively. Additionally, approaches like Dis-PU [18], PU-EVA [24], and MPU [7] have enhanced the PU-Net pipeline by incorporating cascading refinement architectures. Other methods, such as PUGeo-Net [31], NePs [10], and MAFU [32], employ local geometry projections into 2D space to model the underlying 3D surface. More recent approaches have reframed up-sampling as a generation task. For instance, PU-GAN [17] and PUFA-GAN [20] leverage generative adversarial networks (GANs) to

produce high-resolution point clouds. Grad-PU [11] first generates coarse dense point clouds through nearest-point interpolation and then refines them iteratively using diffusion models. In contrast, PUDM [34] directly utilizes conditional diffusion models, treating sparse point clouds as input conditions for generating denser outputs. In this work, our generative model, PointARU, incorporates up-sampling networks in both training stages, making it well-suited for enhancing downstream point cloud up-sampling tasks.

### 3. Method

#### 3.1. Problem Formulation

A point cloud is represented as a set of  $N$  points  $\mathbf{X} = \{\mathbf{x}_i\}_{i=1}^N$ , where each point  $\mathbf{x}_i \in \mathbb{R}^3$  corresponds to a 3D coordinate. As discussed earlier, we model autoregressive point cloud generation using a next-scale prediction approach. The first crucial step in this process is obtaining a sequence of discrete tokens,  $Q = \{q_k\}_{k=1}^K$ , across  $K$  resolution scales to represent different levels of detail in the point cloud  $\mathbf{X}$ . Each scale token  $q_k \in [V]^{s_k}$  contains  $s_k$  integer index tokens, corresponding to  $s_k$  latent point embeddings  $\mathbf{z}_k \in \mathbb{R}^{s_k \times d}$  derived from a learnable codebook  $Z$  with vocabulary size  $V$ . The point cloud  $\mathbf{X}$  is then generated by progressively following the sequence  $Q$ , starting from the coarsest scale  $q_1$  (with the smallest  $s_1$  tokens) and refining up to the finest scale  $q_K$  (with the largest  $s_K$  tokens), adhering to the following probability distribution:

$$p(q_1, q_2, \dots, q_K) = \prod_{k=1}^K p(q_k | q_{k-1}, \dots, q_2, q_1). \quad (1)$$

Since we employ a per-point tokenization strategy,  $s_1 = 1$  represents a single starting point, while  $s_K = N$  corresponds to the total number of points in  $\mathbf{X}$ . The point cloud generation process, as described in Eq. 1, can be interpreted as an autoregressive up-sampling procedure with sequential up-sampling rates  $r_1, r_2, \dots, r_{K-1}$ , satisfying the relationship  $r_{K-1} \dots r_2 r_1 s_1 = s_K = N$ .

#### 3.2. Multi-scale VQVAE for Point Clouds

To obtain the sequence  $Q$ , we utilize a multi-scale residual vector quantization technique to reconstruct the point cloud  $\mathbf{X}$ . The multi-scale VQVAE autoencoder consists of three key modules: (1) Feature Extraction & Down-sampling, (2) Multi-scale Residual Vector Quantization, and (3) Up-sampling & Reconstruction.

**Feature Extraction & Down-sampling.** To extract the latent features  $f$  from the input point cloud  $\mathbf{X}$ , we first convert  $\mathbf{X}$  into a voxel grid representation, denoted as  $\mathbf{V} \in \mathbb{R}^{L \times L \times L \times d}$ , where  $L$  represents the volume size and  $d$  denotes the channel size. A detailed description of the vox-

---

**Algorithm 1** Multi-scale VQVAE encoder for 3D point cloud representations

---

```

1: Input: 3D point cloud  $\mathbf{X} = \{\mathbf{x}_i\}_{i=1}^N$ .
2: Hyperparameters: steps  $K$ , scales  $\{s_k\}_{k=1}^K$ .
3:  $f = \mathcal{E}(\mathbf{X})$ ,  $Q = []$ ;
4: for  $k = 1, \dots, K$  do
5:    $q_k = \mathcal{Q}(\text{down-sampling}(\mathbf{X}, f, s_k))$ 
6:    $Q = \text{queue\_push}(Q, q_k)$ 
7:    $\mathbf{z}_k = \text{lookup}(Z, q_k)$ 
8:    $\mathbf{z}_k = \text{up-sampling}(\mathbf{z}_k, s_K)$ 
9:    $f = f - \phi_k(\mathbf{z}_k)$ 
10: end for
11: Return: a sequence of multi-scale tokens  $Q$ .
```

---



---

**Algorithm 2** Multi-scale VQVAE decoder for 3D point cloud reconstructions

---

```

1: Input: multi-scale tokens  $Q$ .
2: Hyperparameters: steps  $K$ , scales  $\{s_k\}_{k=1}^K$ .
3:  $\hat{f} = 0$ 
4: for  $k = 1, \dots, K$  do
5:    $q_k = \text{queue\_pop}(Q)$ 
6:    $\mathbf{z}_k = \text{lookup}(Z, q_k)$ 
7:    $\mathbf{z}_k = \text{up-sampling}(\mathbf{z}_k, s_K)$ 
8:    $\hat{f} = \hat{f} + \phi_k(\mathbf{z}_k)$ 
9: end for
10:  $\hat{\mathbf{X}} = \mathcal{D}(\hat{f})$ 
11: Return: reconstructed point cloud  $\hat{\mathbf{X}}$ 
```

---

elization process is provided in the appendix. Next, we refine the voxelized features  $\mathbf{V}$  using the PVCNN [21] and query  $\mathbf{V}$  with the original point cloud  $\mathbf{X}$  to obtain the encoded features  $f \in \mathbb{R}^{N \times d}$ . These extracted features serve as input for subsequent multi-scale reconstruction learning. At each scale  $k$ , we apply the farthest point sampling algorithm [9] to generate a sparser point cloud, denoted as  $\mathbf{X}_k \in \mathbb{R}^{s_k \times 3}$  consisting of  $s_k$  points. We then use  $\mathbf{X}_k$  to query the voxel grid  $\mathbf{V}$ , obtaining its corresponding latent representations  $f_k \in \mathbb{R}^{s_k \times d}$ . Notably, since the FPS algorithm does not have a fixed starting point, the sampled points in  $\mathbf{X}_k$  vary during training. This inherent stochasticity enhances model generalization, as it can be viewed as a form of data augmentation for each scale.

**Multi-scale Residual Vector Quantization.** Following the above down-sampling operation, we could obtain the latent features  $f_k$  of each down-sampled point cloud  $\mathbf{X}_k$ , forming a sequence of latent features  $\{f_k\}_{k=1}^K$ . To better reconstruct the original  $f$ , we adopt the residual vector quantization technique that gradually approximates  $f$  in a residual style. First, we convert each latent feature  $f_k$  to the scale token  $q_k \in [V]^{s_k}$  through quantization operation  $\mathcal{Q}$  such that

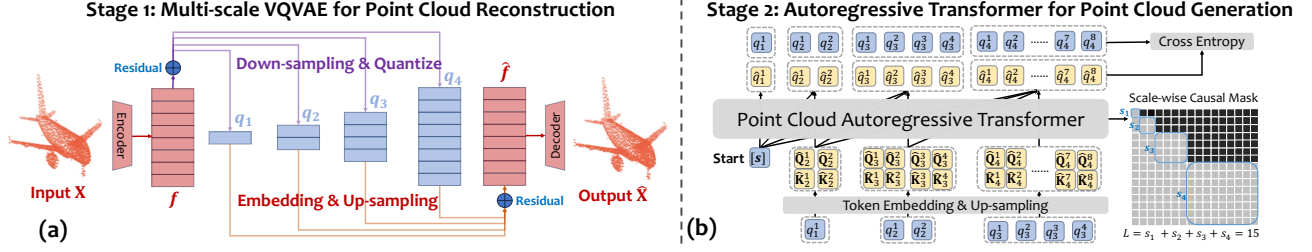


Figure 3. (a) Illustration of training a multi-scale VQ-VAE for point cloud reconstruction, where a multi-scale token sequence  $Q = \{q_1, q_2, q_3, q_4\}$  is obtained with scale sizes  $s_1 = 1, s_2 = 2, s_3 = 4, s_4 = 8$ ; (b) Illustration of training an autoregressive transformer for point cloud generation, following the distribution  $p(q_1, q_2, q_3, q_4) = \prod_{k=1}^4 p(q_k | q_{k-1}, \dots, q_2, q_1)$ , while incorporating a scale-wise attention masking strategy and adhering to the next-scale prediction paradigm.

$q_k = \{q_k^1, q_k^2, \dots, q_k^{s_k}\} = \mathcal{Q}(f_k)$  where each entry  $q_k^i$  is a quantized integer index. Each code index  $q_k^i$  maps its corresponding latent point feature  $f_k^i$  to its nearest embedding vector in the codebook  $Z$  by Euclidean sense:

$$q_k^i = \arg \min_{v \in [v]} \|z_v^i - f_k^i\|_2, \quad (2)$$

where  $z_v^i$  denotes the  $v$ -th embedding vector in the learnable codebook  $Z$  to approximate  $f_k^i$ . In this way, we could obtain the set of scale tokens  $\{q_1, q_2, \dots, q_K\}$  with corresponding scale latent embeddings  $\{z_1, z_2, \dots, z_K\}$ . Then the original  $f$  is approximated in the following residual manner:

$$f[k] = f[k-1] - \phi_k(\text{up-sampling}(z_k, s_K)), \quad (3)$$

where  $f[k]$  denotes the residual feature  $f$  at iteration  $k$  and  $f[0] = f$ . Here  $\phi_k(\cdot)$  denotes the PVCNN network for each iteration/scale  $k$  that refine the up-sampled latent embedding. The up-sampling( $\cdot, s_K$ ) module consists of a series of reshaping operations to increase the latent  $z_k$  to size  $s_K \times d$ , which will be described in the following. We then define the partial sum  $\hat{f}$  as follows:

$$\hat{f} = \sum_{k=1}^K \phi_k(\text{up-sampling}(z_k, s_K)), \quad (4)$$

where  $\hat{f}$  is the final quantized vector of  $f$ . The pseudo-algorithm describing the above encoder and decoder mechanism is shown in Algorithm 1 and Algorithm 2 respectively.

**Up-sampling & Reconstruction.** The up-sampling operation in both Eq. 3 and Eq. 4 follows a PU-Net [45] like operation, which consists of the duplicating and reshaping:

$$z_k(s_k \times d) \xrightarrow{\text{duplicate}} z_k(s_k \times r \times d) \xrightarrow{\text{reshape}} z_k((s_k * r) \times d), \quad (5)$$

where the up-sampling rate  $r = \frac{s_K}{s_k}$  can be pre-computed since both the target size  $s_K$  and the current size  $s_k$  are

known parameters. This up-sampling operation does not rely on the original  $X$ , which can be used to decode intermediate structures in the second stage training. To reconstruct  $X$ , we apply a decoder  $D$  to partial sum  $\hat{f}$  with simple MLP architecture  $\hat{X} = D(\hat{f})$ . The reconstruction loss function to be minimized is as follows:

$$L_{\text{recon}} = L_{\text{CD}}(X, \hat{X}) + L_{\text{EMD}}(X, \hat{X}) + \|sg[f] - z\|_2^2 \quad (6)$$

where  $L_{\text{CD}}$  denotes the chamfer distance loss,  $L_{\text{EMD}}$  denotes the earth-mover distance loss. We inherit these two loss terms from LION [46].  $sg[\cdot]$  is the stop-gradient operation, which ensures that the latent features  $f$  used for reconstruction are consistent with the quantized latent vectors  $z$ , promoting stable and accurate reconstructions. We use exponential moving average (EMA)[3] to maintain the embeddings in the codebook  $Z$ . For all scales, we share the same codebook  $Z$ . The Multi-scale VQVAE is illustrated in Figure 4 (a).

### 3.3. Stage 2: Autoregressive Transformer for Point Cloud Generation

In the second stage, we train an autoregressive point cloud transformer to approximate the distribution in Eq. 1 using the sequence of scale tokens  $Q$  obtained from the previous stage. The transformer consists of two key components: (1) Token embedding layers and (2) Attention mechanisms.

**Token Embedding Layer.** The token pair embedding operation transforms each index token  $q_k^i$  back into a continuous latent embedding. Each token  $q_k^i$  is associated with three key latent embeddings: the codebook embedding  $z_k^i$ , the 3D positional embedding  $p_k^i$  and the scale embedding  $s_k^i$ . The codebook embedding  $z_k^i$  can be easily retrieved from the codebook  $Z$  by querying the token indices:  $z_k^i = \text{look-up}(Z, q_k^i)$ . For positional encoding, we adopt the 3D absolute positional encoding strategy from TIGER [35]. However, this introduces a challenge, as the operation requires explicit 3D point positions as input, yet no explicit



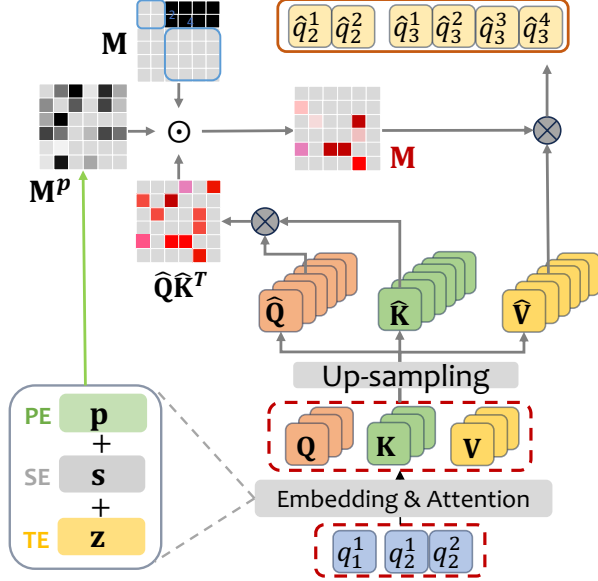


Figure 4. The point cloud autoregressive transformer architecture illustrated by a simpler case containing three scale tokens with scale sizes  $s_1 = 1, s_2 = 2, s_3 = 4$ .

intermediate point cloud structures are available for each set of scale tokens. To address this issue, we decode the intermediate structure  $\hat{\mathbf{X}}_k$  from accumulated predicted tokens up to the  $k$ -th scale  $\{\hat{q}_1, \hat{q}_2, \dots, \hat{q}_k\}$ :

$$\{\hat{\mathbf{z}}_1, \hat{\mathbf{z}}_2, \dots, \hat{\mathbf{z}}_k\} = \text{lookup}(Z, \{\hat{q}_1, \hat{q}_2, \dots, \hat{q}_k\}) \quad (7)$$

$$\hat{\mathbf{X}}_k = D\left(\sum_{k=1}^k \phi_k(\text{up-sampling}(\hat{\mathbf{z}}_k, s_k))\right). \quad (8)$$

In this way, we can derive the absolute positional encoding  $\mathbf{p}_k^i$  for each token  $q_k^i$  with input predicted  $\hat{\mathbf{X}}_k$ . The detailed absolute positional encoding formula is shown in supplementary material. Additionally, the model needs to know which scale that each token belongs to. Therefore,  $\mathbf{s}_k$  is a simple one-hot encoding  $\mathbf{s}_k = \text{one-hot}(k)$  out of total  $K$  scales. Tokens from the same scale ( $q_k^i, q_k^j$ ) share the same scale embedding  $\mathbf{s}_k$ . Following the implementation of Llama 3 [8], we add both positional embedding  $\mathbf{p}_k^i$  and the scale embedding  $\mathbf{s}_k^i$  to the query  $\mathbf{Q}_k^i$  and key vectors  $\mathbf{K}_k^i$  derived in the attention mechanism. Then the token embedding operation for each token  $q_k^i$  is as follows:

$$\mathbf{Q}_k^i = \mathbf{W}_Q \mathbf{z}_k^i + \mathbf{p}_k^i + \mathbf{s}_k^i, \mathbf{K}_k^i = \mathbf{W}_K \mathbf{z}_k^i + \mathbf{p}_k^i + \mathbf{s}_k^i, \quad (9)$$

where  $\mathbf{W}_Q$  and  $\mathbf{W}_K$  are projection matrices for queries  $\mathbf{Q}_k^i$  and keys  $\mathbf{K}_k^i$  respectively. Here, we slightly abuse the notation to align with the conventional representations of queries and keys. Then the input queries and keys will be up-sampled to  $\{\hat{\mathbf{Q}}_k^i, \hat{\mathbf{K}}_k^i\}_{i=1}^{s_{k+1}}$  following the Eq. 5.

**Attention Mechanism.** Compared to the standard attention mechanism, our approach incorporates two key modifications: scale-wise attention and position-aware local attention. Let  $\mathbf{M} \in \mathbb{R}^{s_{\text{total}} \times s_{\text{total}}}$  be the global masking matrix, where  $s_{\text{total}} = s_1 + \dots + s_K$ . The model must be informed that each scale token  $q_k$  is generated only based on the previously generated tokens  $q_1, \dots, q_{k-1}$ . To achieve this, we construct  $\mathbf{M}$  as a block diagonal matrix, where the diagonal blocks  $\mathbf{M}_k$  of size  $s_k \times s_k$  are fully unmasked:  $\mathbf{M} = \text{diag}[\mathbf{M}_1, \mathbf{M}_2, \dots, \mathbf{M}_K]$ . This design allows all tokens within each scale  $k$ , i.e.,  $q_k^1, \dots, q_k^{s_k}$ , to freely attend to one another, as they are generated simultaneously at the same scale. Additionally,  $\mathbf{M}$  retains a lower-triangular structure, adhering to the standard causal masking strategy used in LLM attention mechanisms. This ensures that each token can only attend to previously generated tokens, strictly preventing any access to future tokens.

To effectively capture interactions among tokens  $\{q_k^1, \dots, q_k^{s_k}\}$ , we apply a position-aware soft masking matrix  $\mathbf{M}_k^p$  to integrate the relative positions of token pairs as an informative prior, enhancing the learning of spatial dependencies within the attention mechanism. Specifically,  $\mathbf{M}_k^p$  is derived from the positional embedding matrix  $\mathbf{P}_k \in \mathbb{R}^{s_k \times d}$ , as follows:

$$\mathbf{M}_k^p = \text{Softmax}((\mathbf{P}_k \mathbf{W}_p)(\mathbf{P}_k \mathbf{W}_p)^T), \quad (10)$$

where  $\mathbf{W}_p$  denotes the projection matrix. Each block diagonal matrix  $\mathbf{M}_k$  is then refined by incorporating position-aware soft masking  $\mathbf{M}_k^p$ , ensuring that  $\mathbf{M}_k = \mathbf{M}_k \odot \mathbf{M}_k^p$  where  $\odot$  is the element-wise product operation.

Finally, the output embeddings are passed through a classification layer to predict the tokens  $\{\hat{q}_1, \dots, \hat{q}_K\}$ . The prediction of each token is evaluated using the cross-entropy (CE) loss  $\mathcal{L}_k^i$ , leading to the total loss formulation:

$$\mathcal{L}_{\text{seq}} = \frac{1}{K} \sum_{k=1}^K \mathcal{L}_k, \mathcal{L}_k = \frac{1}{s_k} \sum_{i=1}^{s_k} \mathcal{L}_k^i, \mathcal{L}_k^i = \text{CE}(\hat{q}_k^i, q_k^i) \quad (11)$$

The above Eq. 11 first compute the average loss over all tokens within each scale and get the total sequence prediction loss  $\mathcal{L}_{\text{seq}}$  by averaging all scales. The autoregressive point cloud transformer is illustrated in Figure 4 (b).

## 4. Experiments

### 4.1. Experimental Setup

**Datasets.** In line with prior studies, we have selected ShapeNetv2, pre-processed by PointFlow [44], as our primary dataset. To ensure a fair comparison with various baseline methods, we focus our training and evaluation on three categories: airplanes, chairs, and cars. For each shape, we globally normalize a sample of 2048 points across the entire dataset. The training set comprises 2832 airplanes,

Model	Generative Model	Airplane		Chair		Car		Mean CD ↓	Mean EMD ↓
		CD ↓	EMD ↓	CD ↓	EMD ↓	CD ↓	EMD ↓		
1-GAN [1]	GAN	87.30	93.95	68.58	83.84	66.49	88.78	74.12	88.86
PointFlow [44]	Normalizing Flow	75.68	70.74	62.84	60.57	58.10	56.25	65.54	62.52
DPF-Net [15]	Normalizing Flow	75.18	65.55	62.00	58.53	62.35	54.48	66.51	59.52
SoftFlow [13]	Normalizing Flow	76.05	65.80	59.21	60.05	64.77	60.09	66.67	61.98
SetVAE [14]	VAE	75.31	77.65	58.76	61.48	59.66	61.48	64.58	66.87
ShapeGF [2]	Diffusion	80.00	76.17	68.96	65.48	63.20	56.53	70.72	66.06
DPM [25]	Diffusion	76.42	86.91	60.05	74.77	68.89	79.97	68.45	80.55
PVD-DDIM [36]	Diffusion	76.21	69.84	61.54	57.73	60.95	59.35	66.23	62.31
PSF [40]	Diffusion	<u>71.11</u>	<u>61.09</u>	58.92	54.45	57.19	56.07	62.41	57.20
PVD [49]	Diffusion	73.82	64.81	56.26	53.32	54.55	53.83	61.54	57.32
LION [46]	Diffusion	72.99	64.21	55.67	53.82	53.47	53.21	61.75	57.59
DIT-3D [27]	Diffusion	-	-	<u>54.58</u>	53.21	-	-	-	-
TIGER [35]	Diffusion	73.02	64.10	55.15	53.18	53.21	53.95	60.46	57.08
PointGrow [37]	Autoregressive	82.20	78.54	63.14	61.87	67.56	65.89	70.96	68.77
CanonicalVAE [6]	Autoregressive	80.15	76.27	62.78	61.05	63.23	61.56	68.72	66.29
PointGPT [5]	Autoregressive	74.85	65.61	57.24	55.01	55.91	54.24	63.44	62.24
PointARU-s (ours)	Autoregressive	72.92	63.98	54.89	<u>53.02</u>	<u>52.86</u>	<u>52.07</u>	<u>60.22</u>	<u>56.36</u>
PointARU-m (ours)	Autoregressive	<b>72.24</b>	<b>63.69</b>	<b>54.54</b>	<b>52.85</b>	<b>52.17</b>	<b>51.85</b>	<b>59.65</b>	<b>56.13</b>

Table 1. The *Performance* (1-NNA) is evaluated based on single-class generation. The second block specifies the types of generative models used in each study. The best performance is highlighted in bold, while the second-best performance is underlined.

Model	Training Time (GPU hours) ↓	Sampling Time (s) ↓	Param (M) ↓
PVD [49]	142	29.9	45
LION [46]	550	31.2	60
TIGER [35]	164	23.6	55
PointGrow [37]	156	5.80	25
CanonicalVAE [6]	142	5.45	30
PointGPT [5]	185	5.32	46
PointARU-s (ours)	125	<u>3.21</u>	22
PointARU-m (ours)	178	<u>3.59</u>	32

Table 2. Training time (in GPU hours), sampling time (in seconds), and model size (in millions of parameters). The reported training time is averaged across three categories: airplane, chair, and car, while the sampling time is averaged over all predictions.

4612 chairs, and 2458 cars, while the evaluation set includes 405 airplanes, 662 chairs, and 352 cars.

**Metrics.** In line with the benchmarks established by PVD [49] and LION [46], we adopt the 1-NN (1-nearest neighbor) accuracy [23] as our evaluation criterion. This metric has demonstrated its effectiveness in assessing both the quality and diversity of the generated point clouds, with a score approaching 50% indicating exceptional performance [44]. To calculate the 1-NN distance matrix, we employ two widely recognized metrics for measuring the distance between point clouds: Chamfer Distance (CD) and Earth Movers’ Distance (EMD). We also present the mean CD and the mean EMD by calculating the average CD and EMD across three distinct categories. To assess efficiency, we evaluate the training time by documenting the GPU hours and gauge the sampling efficiency by reporting the average inference time over 10 randomly generated samples.

## 4.2. Performance Comparison for Single-class Generation

**Results.** To evaluate the performance of PointARU, we compare it against several key baseline models, following prior studies. Specifically, we include state-of-the-art (SoTA) diffusion-based models: DPM [25], PVD [49], LION [46], DIT-3D [27], and TIGER [35]. Additionally, we consider PSF [40] and PVD-DDIM [36], which aim to enhance the sampling speed of PVD. Since LION [46] employs a different data split, we re-evaluate it using the conventional split for a fair comparison. Furthermore, we include three prominent autoregressive approaches: PointGrow [37], CanonicalVAE [6], and PointGPT [5]. We report results for two variants of our model, PointARU-s and PointARU-m, representing small and medium parameter sizes, respectively. As shown in Table 1, PointARU significantly outperforms all baseline generative models, achieving SoTA generation quality in both CD and EMD scores. Notably, even PointARU-s delivers remarkable performance, highlighting PointARU’s strong potential for scaling to larger datasets.

**Efficiency.** Table 2 presents the training time, sampling time, and number of parameters for several strong baseline models from Table 1, including PVD, LION, TIGER, and PointGPT. In terms of training efficiency, PointARU-s achieves the shortest training time among all selected methods, while PointARU-m demonstrates comparable training costs to state-of-the-art diffusion-based approaches. For inference efficiency, both PointARU-s and PointARU-m outperform baseline methods with significantly faster sampling

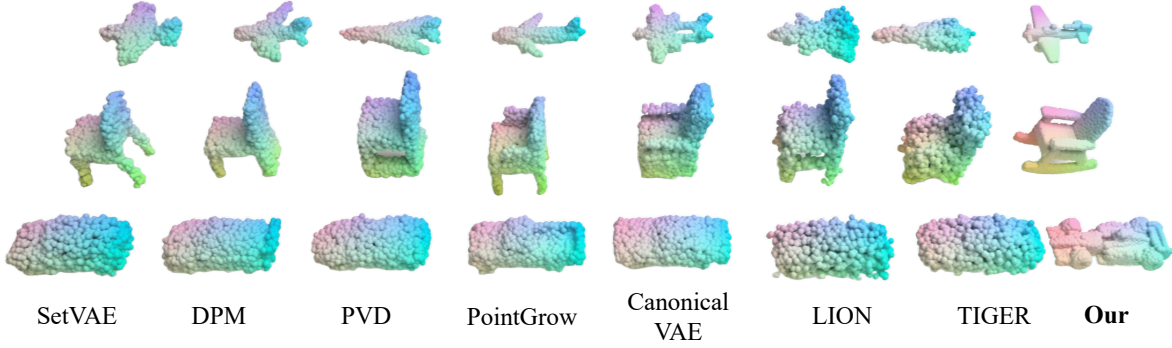


Figure 5. Our generation results (right) compared to baseline models (left). PointARU generates high-quality and diverse 3D point clouds.

speeds. This advantage is primarily due to PointARU’s parallel token generation within each scale. Additionally, PointARU exhibits the highest parameter efficiency among all compared approaches. Notably, PointARU-s has a smaller parameter size than PointGrow, despite the latter performing significantly worse in generation quality. Compared to diffusion-based methods, PointARU-m offers a substantial advantage in parameter efficiency, requiring nearly half the number of parameters while maintaining superior performance.

### 4.3. Ablation and Analysis

Mask	Up-sampling		Aug	TE	Mean CD ↓	Mean EMD ↓
	Voxel	PU-Net				
		✓		SE	64.25	60.53
✓		✓		SE+AbsolutePE	62.19	58.23
✓	✓			SE+AbsolutePE	63.05	58.47
✓		✓		LearnablePE	63.22	59.71
✓		✓		AbsolutePE	62.12	60.03
✓		✓	✓	AbsolutePE	61.28	57.32
✓		✓	✓	SE+LearnablePE	60.62	57.34
✓		✓	✓	SE+AbsolutePE	<b>59.65</b>	<b>56.13</b>

Table 3. Ablation studies on the Transformer backbones, up-sampling networks, token embedding, and trajectory augmentation strategies employed in the second stage of training.

**Neural Architectures & Training Strategies** We also conduct ablation studies to evaluate the impact of various architectural components and training strategies. First, we examine the choice of up-sampling strategy by comparing two primary approaches: *voxel representations* and the *PU-Net strategy*. Our experiments demonstrate that the PU-Net method consistently outperforms voxel-based up-sampling in both CD and EMD metrics. Second, we assess the effectiveness of the *position-aware masking* strategy. The results indicate that this masking mechanism significantly enhances model performance by leveraging relative distance inductive bias, thereby improving learning efficiency given the current dataset scale. Third, we evaluate the contribution of each embedding module within the token embed-

ding (TE) layer. Empirical results highlight the effectiveness of *scale embedding* in particular. We also investigate whether *learnable positional encoding (PE)* or *absolute PE* is more beneficial. Our findings suggest that absolute PE outperforms learnable PE. Finally, we analyze the impact of stochastic trajectory sampling (*aug*), introduced by the inherent stochasticity of the Farthest Point Sampling (FPS) algorithm. To test this, we compare a variant where the starting point of FPS is fixed, ensuring a deterministic trajectory for each training sample. Results clearly show that fixing the trajectory negatively affects generalization, as the up-sampling pathway leading to each shape is inherently non-unique. The results of these ablation studies are summarized in Table 3.

### 4.4. Multi-class Generation

Unlike the single-class generation setting, we further evaluate all models on the more challenging multi-class generation task inherited from LION [46] to assess their cross-category learning capability. We train PointARU and other baselines with class conditioning on a diverse set of 55 distinct categories from ShapeNet. This conditional formulation enables the model to learn class-specific features while simultaneously leveraging shared geometric patterns across categories. The model can disentangle class-specific attributes from common structural properties by incorporating class information as an explicit conditioning signal, thereby enhancing its generative capabilities across the diverse shape taxonomy. As shown in Table 4, PointARU still outperforms all selected strong baselines.

### 4.5. Point Cloud Completion & Up-sampling

We evaluate PointARU on two key downstream tasks: point cloud completion and point cloud up-sampling. For point cloud completion, we follow the problem setting from PVD [49]. For point cloud up-sampling, we set the up-sampling rate to  $r = 2$ , increasing 2048 points to denser 4096 points. As shown in Table 5, PointARU consistently achieves the

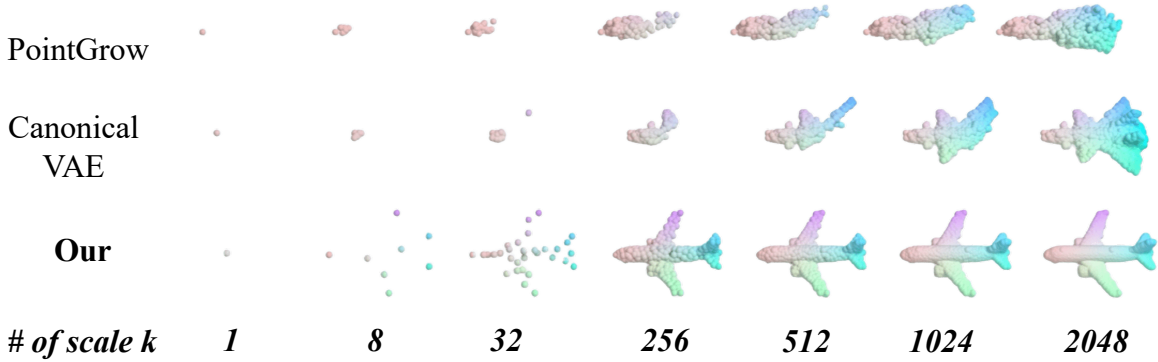


Figure 6. An illustration and comparison of the autoregressive generation process across three approaches: PointGrow, Canonical VAE, and PointARU. Unlike previous approaches, PointARU leverages the next-scale prediction paradigm, enabling it to establish the backbone of shapes early in the generation process.

	Airplane		Chair		Car	
	CD ↓	EMD ↓	CD ↓	EMD ↓	CD ↓	EMD ↓
PVD	97.53	99.88	88.37	96.37	89.77	94.89
TIGER	83.54	81.55	<u>57.34</u>	61.45	65.79	57.24
PointGPT	94.94	91.73	71.83	79.00	89.35	87.22
LION	86.30	77.04	66.50	63.85	64.52	54.21
PointARU-s (ours)	<u>78.95</u>	68.84	58.79	<u>55.10</u>	<u>59.97</u>	<u>52.89</u>
PointARU-m (ours)	<b>75.42</b>	<b>66.54</b>	<b>56.03</b>	<b>52.22</b>	<b>57.95</b>	<b>49.55</b>

Table 4. Generation results (1-NNA↓) on ShapeNet dataset from PointFlow. All data normalized individually into [-1, 1].

best EMD score in the point cloud completion task, though it underperforms some earlier baselines in CD score, highlighting potential areas for improvement. For the up-sampling task, PointARU surpasses all selected baselines, demonstrating strong generalization capabilities. Visualization results for both tasks are presented in Figure 7.

Category	Model	CD ↓	EMD ↓	Category	Model	CD ↓	EMD ↓
Airplane	SoftFlow	40.42	11.98	Airplane	PVD	73.56	71.65
	PointFlow	<b>40.30</b>	11.80		TIGER	71.65	59.94
	DPF-Net	52.79	11.05		PointGPT	72.11	60.12
	PVD	44.15	<u>10.30</u>		LION	<u>70.41</u>	59.65
	PointARU-m (ours)	42.02	<b>10.15</b>		PointARU-m (ours)	<b>68.89</b>	<b>58.86</b>
Chair	SoftFlow	27.86	32.95	Chair	PVD	53.81	64.61
	PointFlow	<b>27.07</b>	36.49		TIGER	<u>52.80</u>	<u>52.98</u>
	DPF-Net	<u>27.63</u>	33.20		PointGPT	53.75	53.21
	PVD	32.11	<u>29.39</u>		LION	53.98	54.33
	PointARU-m (ours)	28.51	<b>29.83</b>		PointARU-m (ours)	<b>52.04</b>	<b>51.03</b>
Car	SoftFlow	18.50	27.89	Car	PVD	58.95	48.43
	PointFlow	18.03	28.51		PointGPT	57.26	47.85
	DPF-Net	<b>13.96</b>	23.18		TIGER	57.90	48.01
	PVD	17.74	<u>21.46</u>		LION	<u>57.14</u>	47.56
	PointARU-m (ours)	<u>16.25</u>	<b>20.71</b>		PointARU-m (ours)	<b>55.85</b>	<b>46.74</b>

Table 5. (Left) The shape completion task in PVD. (Right) Our own up-sampling task by up-sampling to denser point clouds.

## 5. Conclusions

In this study, we introduce PointARU, a groundbreaking autoregressive generation paradigm for high-quality 3D point cloud generation. Unlike previous autoregressive

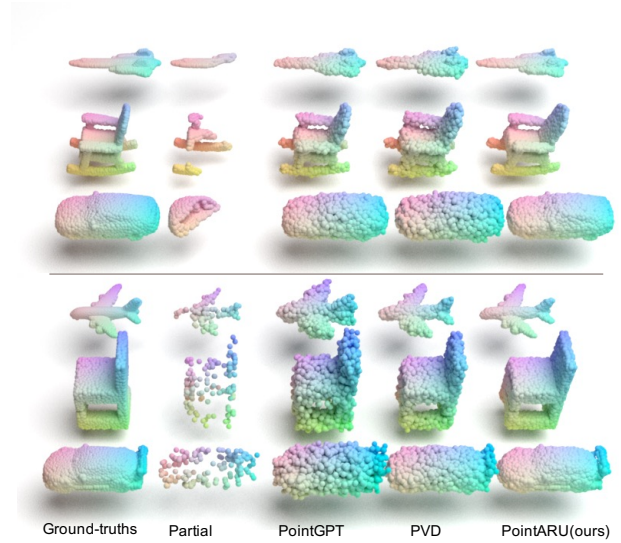


Figure 7. Shape completion (Upper) and up-sampling (Lower) visualization. From left to right: ground-truth shapes, partial shapes sampled from ground-truth, baselines, and our results.

methods, PointARU adopts a coarse-to-fine autoregressive up-sampling approach, eliminating the need to define a fixed generation order for point sequences. Our method significantly surpasses existing point cloud generative models in both generation quality and parameter efficiency while also demonstrating superior performance in downstream tasks such as point cloud completion and up-sampling. For future work, we aim to explore advanced training strategies to further enhance the performance of PointARU. Additionally, integrating PointARU with diffusion-based approaches presents another promising research direction.



## References

- [1] Panos Achlioptas, Olga Diamanti, Ioannis Mitliagkas, and Leonidas J. Guibas. Learning representations and generative models for 3d point clouds. In *Proceedings of the 35th International Conference on Machine Learning, ICML 2018, Stockholmsmässan, Stockholm, Sweden, July 10-15, 2018*, pages 40–49. PMLR, 2018. 6
- [2] Ruojin Cai, Guandao Yang, Hadar Averbuch-Elor, Zekun Hao, Serge J. Belongie, Noah Snavely, and Bharath Hariharan. Learning gradient fields for shape generation. In *Computer Vision - ECCV 2020 - 16th European Conference, Glasgow, UK, August 23-28, 2020, Proceedings, Part III*, pages 364–381. Springer, 2020. 2, 6
- [3] Zhaowei Cai, Avinash Ravichandran, Subhransu Maji, Charless Fowlkes, Zhuowen Tu, and Stefano Soatto. Exponential moving average normalization for self-supervised and semi-supervised learning. In *Proceedings of the IEEE/CVF Conference on Computer Vision and Pattern Recognition*, pages 194–203, 2021. 4
- [4] Huiwen Chang, Han Zhang, Lu Jiang, Ce Liu, and William T. Freeman. Maskgit: Masked generative image transformer. In *IEEE/CVF Conference on Computer Vision and Pattern Recognition, CVPR 2022, New Orleans, LA, USA, June 18-24, 2022*, pages 11305–11315. IEEE, 2022. 1
- [5] Guangyan Chen, Meiling Wang, Yi Yang, Kai Yu, Li Yuan, and Yufeng Yue. Pointgpt: Auto-regressively generative pre-training from point clouds. In *Advances in Neural Information Processing Systems 36: Annual Conference on Neural Information Processing Systems 2023, NeurIPS 2023, New Orleans, LA, USA, December 10 - 16, 2023*, 2023. 1, 2, 6
- [6] An-Chieh Cheng, Xueting Li, Sifei Liu, Min Sun, and Ming-Hsuan Yang. Autoregressive 3d shape generation via canonical mapping. In *Computer Vision - ECCV 2022 - 17th European Conference, Tel Aviv, Israel, October 23-27, 2022, Proceedings, Part III*, pages 89–104. Springer, 2022. 1, 2, 6
- [7] Hang Du, Xuejun Yan, Jingjing Wang, Di Xie, and Shiliang Pu. Point cloud upsampling via cascaded refinement network. In *Computer Vision - ACCV 2022 - 16th Asian Conference on Computer Vision, Macao, China, December 4-8, 2022, Proceedings, Part I*, pages 106–122. Springer, 2022. 2
- [8] Abhimanyu Dubey, Abhinav Jauhri, Abhinav Pandey, Abhishek Kadian, Ahmad Al-Dahle, Aiesha Letman, Akhil Mathur, Alan Schelten, Amy Yang, Angela Fan, Anirudh Goyal, Anthony Hartshorn, Aobo Yang, Archi Mitra, Archie Sravankumar, Artem Korenev, Arthur Hinsvark, Arun Rao, Aston Zhang, Aurélien Rodriguez, Austen Gregerson, Ava Spataru, Baptiste Rozière, Bethany Biron, Binh Tang, Bobbie Chern, Charlotte Caucheteux, Chaya Nayak, Chloe Bi, Chris Marra, Chris McConnell, Christian Keller, Christophe Touret, Chunyang Wu, Corinne Wong, Cristian Canton Ferrer, Cyrus Nikolaidis, Damien Allonsius, Daniel Song, Danielle Pintz, Danny Livshits, David Esiobu, Dhruv Choudhary, Dhruv Mahajan, Diego Garcia-Olano, Diego Perino, Dieuwke Hupkes, Egor Lakomkin, Ehab AlBadawy, Elina Lobanova, Emily Dinan, Eric Michael Smith, Filip Radenovic, Frank Zhang, Gabriel Synnaeve, Gabrielle Lee, Georgia Lewis Anderson, Graeme Nail, Grégoire Mialon, Guan Pang, Guillem Cucurell, Hailey Nguyen, Hannah Korevaar, Hu Xu, Hugo Touvron, Iliyan Zarov, Imanol Arrieta Ibarra, Isabel M. Kloumann, Ishan Misra, Ivan Evtimov, Jade Copet, Jaewon Lee, Jan Geffert, Jana Vranes, Jason Park, Jay Mahadeokar, Jeet Shah, Jelmer van der Linde, Jennifer Billock, Jenny Hong, Jenya Lee, Jeremy Fu, Jianfeng Chi, Jianyu Huang, Jiawen Liu, Jie Wang, Jiecao Yu, Joanna Bitton, Joe Spisak, Jongsoo Park, Joseph Rocca, Joshua Johnstun, Joshua Saxe, Junteng Jia, Kalyan Vasuden Alwala, Kartikeya Upasani, Kate Plawiak, Ke Li, Kenneth Heafield, Kevin Stone, and et al. The llama 3 herd of models. *CoRR*, abs/2407.21783, 2024. 5
- [9] Yuval Eldar, Michael Lindenbaum, Moshe Porat, and Yehoshua Y. Zeevi. The farthest point strategy for progressive image sampling. *IEEE Trans. Image Process.*, 6(9):1305–1315, 1997. 3
- [10] Wanquan Feng, Jin Li, Hongrui Cai, Xiaonan Luo, and Juyong Zhang. Neural points: Point cloud representation with neural fields for arbitrary upsampling. In *IEEE/CVF Conference on Computer Vision and Pattern Recognition, CVPR 2022, New Orleans, LA, USA, June 18-24, 2022*, pages 18612–18621. IEEE, 2022. 2
- [11] Yun He, Danhang Tang, Yinda Zhang, Xiangyang Xue, and Yanwei Fu. Grad-pu: Arbitrary-scale point cloud upsampling via gradient descent with learned distance functions. In *IEEE/CVF Conference on Computer Vision and Pattern Recognition, CVPR 2023, Vancouver, BC, Canada, June 17-24, 2023*, pages 5354–5363. IEEE, 2023. 3
- [12] Zitian Huang, Yikuan Yu, Jiawen Xu, Feng Ni, and Xinyi Le. Pf-net: Point fractal network for 3d point cloud completion. In *2020 IEEE/CVF Conference on Computer Vision and Pattern Recognition, CVPR 2020, Seattle, WA, USA, June 13-19, 2020*, pages 7659–7667. Computer Vision Foundation / IEEE, 2020. 1
- [13] Hyeongju Kim, Hyeonseung Lee, Woo Hyun Kang, Joun Yeop Lee, and Nam Soo Kim. Softflow: Proba-

- bilistic framework for normalizing flow on manifolds. In *Advances in Neural Information Processing Systems 33: Annual Conference on Neural Information Processing Systems 2020, NeurIPS 2020, December 6-12, 2020, virtual*, 2020. 6
- [14] Jinwoo Kim, Jaehoon Yoo, Juho Lee, and Seunghoon Hong. Setvae: Learning hierarchical composition for generative modeling of set-structured data. In *IEEE Conference on Computer Vision and Pattern Recognition, CVPR 2021, virtual, June 19-25, 2021*, pages 15059–15068. Computer Vision Foundation / IEEE, 2021. 6
- [15] Roman Klokov, Edmond Boyer, and Jakob Verbeek. Discrete point flow networks for efficient point cloud generation. In *Computer Vision - ECCV 2020 - 16th European Conference, Glasgow, UK, August 23-28, 2020, Proceedings, Part XXIII*, pages 694–710. Springer, 2020. 6
- [16] Doyup Lee, Chiheon Kim, Saehoon Kim, Minsu Cho, and Wook-Shin Han. Autoregressive image generation using residual quantization. In *IEEE/CVF Conference on Computer Vision and Pattern Recognition, CVPR 2022, New Orleans, LA, USA, June 18-24, 2022*, pages 11513–11522. IEEE, 2022. 1, 2
- [17] Ruihui Li, Xianzhi Li, Chi-Wing Fu, Daniel Cohen-Or, and Pheng-Ann Heng. PU-GAN: A point cloud upsampling adversarial network. In *2019 IEEE/CVF International Conference on Computer Vision, ICCV 2019, Seoul, Korea (South), October 27 - November 2, 2019*, pages 7202–7211. IEEE, 2019. 2
- [18] Ruihui Li, Xianzhi Li, Pheng-Ann Heng, and Chi-Wing Fu. Point cloud upsampling via disentangled refinement. In *IEEE Conference on Computer Vision and Pattern Recognition, CVPR 2021, virtual, June 19-25, 2021*, pages 344–353. Computer Vision Foundation / IEEE, 2021. 2
- [19] Tianhong Li, Yonglong Tian, He Li, Mingyang Deng, and Kaiming He. Autoregressive image generation without vector quantization. *CoRR*, abs/2406.11838, 2024. 1
- [20] Hao Liu, Hui Yuan, Junhui Hou, Raouf Hamzaoui, and Wei Gao. PUFA-GAN: A frequency-aware generative adversarial network for 3d point cloud upsampling. *IEEE Trans. Image Process.*, 31:7389–7402, 2022. 2
- [21] Zhijian Liu, Haotian Tang, Yujun Lin, and Song Han. Point-voxel CNN for efficient 3d deep learning. In *Advances in Neural Information Processing Systems 32: Annual Conference on Neural Information Processing Systems 2019, NeurIPS 2019, December 8-14, 2019, Vancouver, BC, Canada*, pages 963–973, 2019. 3
- [22] Yunfei Long, Daniel Morris, Xiaoming Liu, Marcos Castro, Punarjay Chakravarty, and Praveen Narayanan. Radar-camera pixel depth association for depth completion. In *IEEE Conference on Computer Vision and Pattern Recognition, CVPR 2021, virtual, June 19-25, 2021*, pages 12507–12516. Computer Vision Foundation / IEEE, 2021. 1
- [23] David Lopez-Paz and Maxime Oquab. Revisiting classifier two-sample tests. In *5th International Conference on Learning Representations, ICLR 2017, Toulon, France, April 24-26, 2017, Conference Track Proceedings*. OpenReview.net, 2017. 6
- [24] Luqing Luo, Lulu Tang, Wanyi Zhou, Shizheng Wang, and Zhi-Xin Yang. PU-EVA: an edge-vector based approximation solution for flexible-scale point cloud up-sampling. In *2021 IEEE/CVF International Conference on Computer Vision, ICCV 2021, Montreal, QC, Canada, October 10-17, 2021*, pages 16188–16197. IEEE, 2021. 2
- [25] Shitong Luo and Wei Hu. Diffusion probabilistic models for 3d point cloud generation. In *IEEE Conference on Computer Vision and Pattern Recognition, CVPR 2021, virtual, June 19-25, 2021*, pages 2837–2845. Computer Vision Foundation / IEEE, 2021. 1, 2, 6
- [26] Paritosh Mittal, Yen-Chi Cheng, Maneesh Singh, and Shubham Tulsiani. Autosdf: Shape priors for 3d completion, reconstruction and generation. In *IEEE/CVF Conference on Computer Vision and Pattern Recognition, CVPR 2022, New Orleans, LA, USA, June 18-24, 2022*, pages 306–315. IEEE, 2022. 1
- [27] Shentong Mo, Enze Xie, Ruihang Chu, Lanqing Hong, Matthias Nießner, and Zhenguo Li. Dit-3d: Exploring plain diffusion transformers for 3d shape generation. In *Advances in Neural Information Processing Systems 36: Annual Conference on Neural Information Processing Systems 2023, NeurIPS 2023, New Orleans, LA, USA, December 10 - 16, 2023*, 2023. 6
- [28] OpenAI. GPT-4 technical report. *CoRR*, abs/2303.08774, 2023. 1
- [29] Ajay Patel, Bryan Li, Mohammad Sadegh Rasooli, Noah Constant, Colin Raffel, and Chris Callison-Burch. Bidirectional language models are also few-shot learners. In *The Eleventh International Conference on Learning Representations, ICLR 2023, Kigali, Rwanda, May 1-5, 2023*. OpenReview.net, 2023. 1
- [30] Guocheng Qian, Abdulellah Abualshour, Guohao Li, Ali K. Thabet, and Bernard Ghanem. PU-GCN: point cloud upsampling using graph convolutional networks. In *IEEE Conference on Computer Vision and Pattern Recognition, CVPR 2021, virtual, June 19-25, 2021*, pages 11683–11692. Computer Vision Foundation / IEEE, 2021. 2
- [31] Yue Qian, Junhui Hou, Sam Kwong, and Ying He. Pugeo-net: A geometry-centric network for 3d point cloud upsampling. In *Computer Vision - ECCV 2020*

- *16th European Conference, Glasgow, UK, August 23-28, 2020, Proceedings, Part XIX*, pages 752–769. Springer, 2020. 2
- [32] Yue Qian, Junhui Hou, Sam Kwong, and Ying He. Deep magnification-flexible upsampling over 3d point clouds. *IEEE Trans. Image Process.*, 30:8354–8367, 2021. 2
- [33] Shi Qiu, Saeed Anwar, and Nick Barnes. Pu-transformer: Point cloud upsampling transformer. In *Computer Vision - ACCV 2022 - 16th Asian Conference on Computer Vision, Macao, China, December 4-8, 2022, Proceedings, Part I*, pages 326–343. Springer, 2022. 2
- [34] Wentao Qu, Yuantian Shao, Lingwu Meng, Xiaoshui Huang, and Liang Xiao. A conditional denoising diffusion probabilistic model for point cloud upsampling. In *IEEE/CVF Conference on Computer Vision and Pattern Recognition, CVPR 2024, Seattle, WA, USA, June 16-22, 2024*, pages 20786–20795. IEEE, 2024. 3
- [35] Zhiyuan Ren, Minchul Kim, Feng Liu, and Xiaoming Liu. TIGER: time-varying denoising model for 3d point cloud generation with diffusion process. In *IEEE/CVF Conference on Computer Vision and Pattern Recognition, CVPR 2024, Seattle, WA, USA, June 16-22, 2024*, pages 9462–9471. IEEE, 2024. 1, 2, 4, 6, 13
- [36] Jiaming Song, Chenlin Meng, and Stefano Ermon. Denoising diffusion implicit models. In *9th International Conference on Learning Representations, ICLR 2021, Virtual Event, Austria, May 3-7, 2021*. OpenReview.net, 2021. 2, 6
- [37] Yongbin Sun, Yue Wang, Ziwei Liu, Joshua E. Siegel, and Sanjay E. Sarma. Pointgrow: Autoregressively learned point cloud generation with self-attention. In *IEEE Winter Conference on Applications of Computer Vision, WACV 2020, Snowmass Village, CO, USA, March 1-5, 2020*, pages 61–70. IEEE, 2020. 1, 2, 6
- [38] Keyu Tian, Yi Jiang, Zehuan Yuan, Bingyue Peng, and Liwei Wang. Visual autoregressive modeling: Scalable image generation via next-scale prediction. *CoRR*, abs/2404.02905, 2024. 1
- [39] Haibin Wu, Kai-Wei Chang, Yuan-Kuei Wu, and Hung-yi Lee. Speechgen: Unlocking the generative power of speech language models with prompts. *CoRR*, abs/2306.02207, 2023. 1
- [40] Lemeng Wu, Dilin Wang, Chengyue Gong, Xingchao Liu, Yunyang Xiong, Rakesh Ranjan, Raghuraman Krishnamoorthi, Vikas Chandra, and Qiang Liu. Fast point cloud generation with straight flows. In *IEEE/CVF Conference on Computer Vision and Pattern Recognition, CVPR 2023, Vancouver, BC, Canada, June 17-24, 2023*, pages 9445–9454. IEEE, 2023. 2, 6
- [41] Jianwen Xie, Zilong Zheng, Ruiqi Gao, Wenguan Wang, Song-Chun Zhu, and Ying Nian Wu. Learning descriptor networks for 3d shape synthesis and analysis. In *2018 IEEE Conference on Computer Vision and Pattern Recognition, CVPR 2018, Salt Lake City, UT, USA, June 18-22, 2018*, pages 8629–8638. Computer Vision Foundation / IEEE Computer Society, 2018. 1
- [42] Jinheng Xie, Weijia Mao, Zechen Bai, David Junhao Zhang, Weihao Wang, Kevin Qinghong Lin, Yuchao Gu, Zhijie Chen, Zhenheng Yang, and Mike Zheng Shou. Show-o: One single transformer to unify multi-modal understanding and generation, 2024. 1
- [43] Xingguang Yan, Liqiang Lin, Niloy J. Mitra, Dani Lischinski, Daniel Cohen-Or, and Hui Huang. Shapeformer: Transformer-based shape completion via sparse representation. In *IEEE/CVF Conference on Computer Vision and Pattern Recognition, CVPR 2022, New Orleans, LA, USA, June 18-24, 2022*, pages 6229–6239. IEEE, 2022. 1
- [44] Guandao Yang, Xun Huang, Zekun Hao, Ming-Yu Liu, Serge J. Belongie, and Bharath Hariharan. Pointflow: 3d point cloud generation with continuous normalizing flows. In *2019 IEEE/CVF International Conference on Computer Vision, ICCV 2019, Seoul, Korea (South), October 27 - November 2, 2019*, pages 4540–4549. IEEE, 2019. 2, 5, 6
- [45] Lequan Yu, Xianzhi Li, Chi-Wing Fu, Daniel Cohen-Or, and Pheng-Ann Heng. Pu-net: Point cloud upsampling network. In *2018 IEEE Conference on Computer Vision and Pattern Recognition, CVPR 2018, Salt Lake City, UT, USA, June 18-22, 2018*, pages 2790–2799. Computer Vision Foundation / IEEE Computer Society, 2018. 1, 2, 4
- [46] Xiaohui Zeng, Arash Vahdat, Francis Williams, Zan Gojcic, Or Litany, Sanja Fidler, and Karsten Kreis. LION: latent point diffusion models for 3d shape generation. In *Advances in Neural Information Processing Systems 35: Annual Conference on Neural Information Processing Systems 2022, NeurIPS 2022, New Orleans, LA, USA, November 28 - December 9, 2022*, 2022. 1, 2, 4, 6, 7, 13
- [47] Dong Zhang, Shimin Li, Xin Zhang, Jun Zhan, Pengyu Wang, Yaqian Zhou, and Xipeng Qiu. Speechgpt: Empowering large language models with intrinsic cross-modal conversational abilities. In *Findings of the Association for Computational Linguistics: EMNLP 2023, Singapore, December 6-10, 2023*, pages 15757–15773. Association for Computational Linguistics, 2023. 1
- [48] Chunting Zhou, Lili Yu, Arun Babu, Kushal Tirumala, Michihiro Yasunaga, Leonid Shamis, Jacob Kahn, Xuezhe Ma, Luke Zettlemoyer, and Omer Levy.

Transfusion: Predict the next token and diffuse images with one multi-modal model, 2024. [1](#)

- [49] Linqi Zhou, Yilun Du, and Jiajun Wu. 3d shape generation and completion through point-voxel diffusion. In *2021 IEEE/CVF International Conference on Computer Vision, ICCV 2021, Montreal, QC, Canada, October 10-17, 2021*, pages 5806–5815. IEEE, 2021. [1](#), [2](#), [6](#), [7](#)



## Supplemental Materials for 3D Point Cloud Generation via Autoregressive Up-sampling

### The First Stage Training Details

**Point-Voxel CNN.** We convert the point cloud  $\mathbf{X} = \{\mathbf{x}_i\}_{i=1}^N$  into voxel grids  $\{\mathbf{V}_{u,v,w}\} = \mathbf{V} \in \mathbb{R}^{L \times L \times L \times d}$  by taking the average of all features  $\mathbf{f}_k$ , where the coordinate  $\mathbf{x}_i = (x_i, y_i, z_i)$  is located within the voxel grid  $(u, v, w)$ :

$$\mathbf{V}_{u,v,w,d} = \frac{1}{N_{u,v,w}} \sum_{i=1}^N \mathbb{I}[x_i \in \mathbb{N}(u, \delta), y_i \in \mathbb{N}(v, \delta), z_i \in \mathbb{N}(w, \delta)] \times \mathbf{f}_{k,d}, \quad (12)$$

where  $\mathbb{N}(z, \delta) = \{x | x \in [z - \delta, z + \delta]\}$ ,  $\mathbf{f}_{k,d}$  denotes the  $d$ th channel feature corresponding to  $\mathbf{x}_i$ ,  $N_{u,v,w}$  is the normalization factor (i.e. the number of points that fall in that voxel grid),  $\mathbb{I}(\cdot)$  denotes the binary indicator of whether the  $i$ th point falls into the voxel grid  $(u, v, w)$ . After voxelization, we apply a series of 3D convolution, Swish activation, GroupNorm and Multi-layer Perceptrons (MLP) to further refine the volume features to  $\mathbf{V} \in \mathbb{R}^{L \times L \times L \times d}$ .

### The Second Stage Training Details

**Positional Encoding.** We adopt the absolute positional encoding strategy used in TIGER [35]. Based on our experiments, we find the Base  $\lambda$  Position Encoding (B $\lambda$ PE) performs better and here we present its formula:

$$pos = \lambda^2 * z_i + \lambda * y_i + x_i \quad (13)$$

$$\mathbf{P}_k(pos, 2i) = \sin\left(\frac{pos}{10000^{\frac{2i}{D}}}\right) \quad (14)$$

$$\mathbf{P}_k(pos, 2i + 1) = \cos\left(\frac{pos}{10000^{\frac{2i}{D}}}\right), \quad (15)$$

where  $pos$  is a polynomial expression of  $\lambda$ . We set  $\lambda$  to 1000 following the setting in TIGER [35], which means this preserves three decimal places of precision. Here  $\mathbf{P}_k \in \mathbb{R}^{s_k \times D}$  denotes the positional embedding of all  $s_k$  tokens within the scale  $k$ . In short, we apply the B $\lambda$ PE embedding strategy scale-by-scale at this time.

### Implementation Details, Hyperparameters and Reproducibility Settings

**Hyper-parameters and Reproducibility Settings.** We mainly follow the setting in [46]. Specifically, we set the learning rate  $3e^{-4}$  and the batch-size 32. We perform all the experiments on a workstation with Intel Xeon Gold 6154 CPU (3.00GHz) and 8 NVIDIA Tesla V100 (32GB) GPUs.

Hyperparameter	Value
# PVCNN layers	4
# PVCNN hidden dimension	1024
# PVCNN voxel grid size	32
# MLP layers	6
# Attention dimension	1024
# Attention head	32
Optimizer	AdamW
Weight Decay	0.01
LR Schedule	Cosine

### More Visualization Results on ShapeNetV2

**3D Point Clouds Generated by PointARU.** In the primary experiment, we focus on three typical shapes from the ShapeNetV2 dataset, in line with previous studies. Additionally, we train our model using other shapes from the ShapeNetV2 dataset and display a variety of 3D point clouds, each generated by our method and representing different shapes. The visualization results are shown in Figure S1 and Figure S2.



Figure S1. Generated shapes from the PointARU model trained on ShapeNet's other categories.

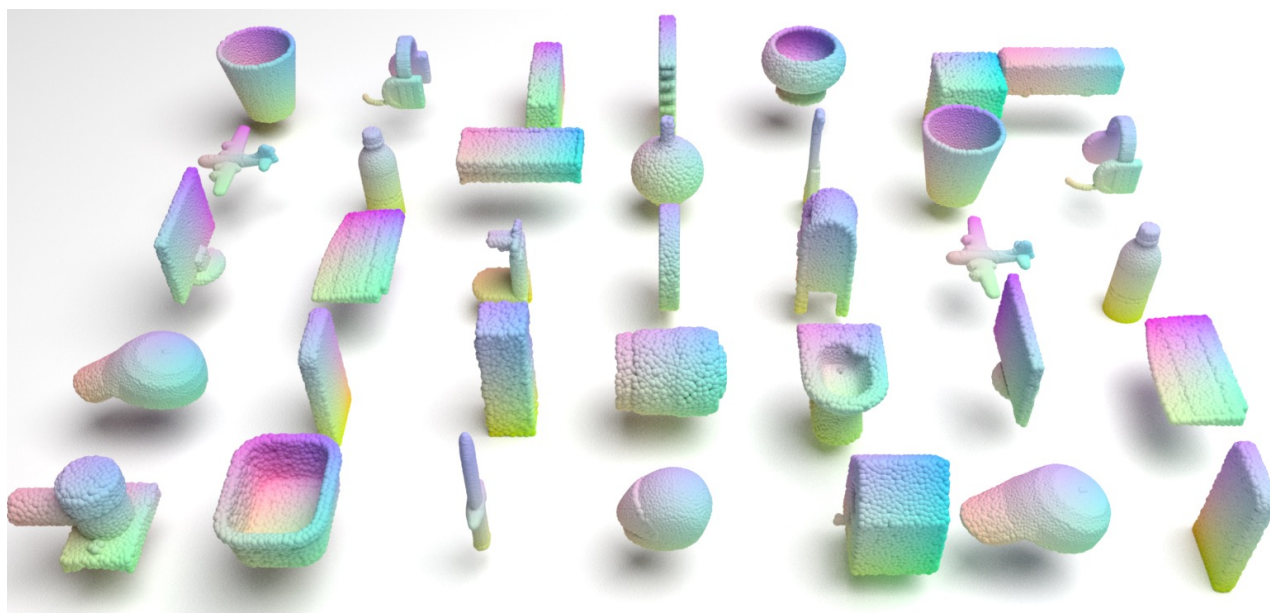


Figure S2. Generated shapes from the PointARU model trained on ShapeNet's other categories.